018530 - SWITCH

Sustainable Water Management in the City of the Future

Integrated Project
Global Change and Ecosystems

Deliverable 2.3.1d – Hydrology of Brown Roofs

Due date of deliverable: January 2011
Actual submission date: June 2011

Start date of project: 1 February 2006 Duration: 60 months

University of Birmingham

Draft Final

Project co-funded by the European Commission within the Sixth Framework Programme (2002-2006)		
Dissemination Level		
PU	Public	
PP	Restricted to other programme participants (including the Commission Services)	
RE	Restricted to a group specified by the consortium (including the Commission Services)	
CO	Confidential, only for members of the consortium (including the Commission Services)	x

Authors: Turner, R., Mackay, R., Bates, A. J. And Cuthbert, M.,
School of Geography Earth and Environmental Sciences, University of Birmingham.

Contents

1 Introduction

Urbanization in most countries has led to an ever larger extent of impervious urban covers, such as roads, pavements, carparks and roofs, which serve to disturb the hydrological cycle, reducing the retention and delay of precipitation runoff by processes such as interception, infiltration and surface ponding. This has in most cases resulted in the intensification of stormwater discharge across the urban landscape (Mentens, 2006; Palla et al., 2009). Increased stormwater, both magnitude and intensity, can negatively impact the urban environment as well as the downstream natural environment. The increase in peak runoff rates associated with high flow volumes in receiving surface water bodies has been linked to channelisation and bank erosion, higher sediment flows and decreases in local biodiversity due to the altered hydrological conditions. Heightened urban runoff has also been shown to increase the risk of pollutant mobility and subsequent contamination of water bodies (Hilten et al., 2008). Impurities such as salt and hydrocarbons from roads find their way into the stormwater network and are subsequently discharged to a water body or leaked to an underlying aquifer. Finally, instances of flooding have increased with greater runoff volumes, and with predicted climate change may further increase the risk of disruption to urban environments by such flood events. As such, an increasing need to implement methods of simulating or imitating natural processes of storage, slow conveyance and gradual release of storm water volumes has been identified as an important feature for inclusion in future urban water management. Many Sustainable Drainage Schemes (SuDS) or Best Management Practices (BMPs) include structures that aim to replicate these natural processes such as swales, detention ponds and green roofs. Green roofs have proved popular because they can be retrofitted to rooftops in metropolitan areas where available land for other SuDS schemes is at a premium. Indeed, rooftops in the urban environment can make up to almost 50% of the total impervious surface area (Carter and Rasmussen, 2006) and so green roofs offer an option to benefit, rather than contribute to, urban stormwater problems.

Green roof research has been an area of study that has received increasing interest over the past decade or so, largely due to the reported wide range of ecological benefits that these structures can provide. They have been reported to increase air quality in built up areas, can provide habitat for more species and therefore improve urban biodiversity, provide mitigation of the urban heat island effect and reduce thermal load and subsequent energy demands for heating or cooling of buildings, attenuation of peak run-off rates and total flow volumes after storm events, along with general aesthetic improvement of the urban environment.

Green roofs are generally categorized as one of two types, an intensive or extensive green roof. Intensive green roofs have a deep substrate layer (>150mm) and are populated by grasses, shrubs and perennial species. They are more likely to require high levels of maintenance and irrigation, and due to the weight of the substrate and plants, these are not easily retrofitted to existing rooftops. Extensive green roofs have shallower substrate layers (<150mm) and are dominated by drought resilient species such as sedums and mosses. They require minimal maintenance and can be retrofitted

to most rooftops and installed on slopes as high as 45^{o} (Mentens, 1999, after Krupka, 1992: Kolb and Schwartz, 1999).

Research into the functioning of green roof systems has produced mixed results. Carter and Rasmussen (2006) reported maximum precipitation retention of just under 90% for small storms and a minimum retention of 50% for storm volumes of greater than 7.62 cm. They also recorded an average increase in the lag between peak precipitation and peak runoff of, on average, 34.9 minutes, 17.9 minutes greater than that displayed by black roofs in their study. Villlarreal (2006) reports maximum values of 52% retention for variable rainfall intensities, but for constant rainfall events the maximum retention volume decreased to 29%. Spolek (2008) discovered that over a 3 year period of monitoring a green roof in Portland, Oregon rainwater discharge was reduced by 25%. As observed by Hilten (2008) and Carter and Rasmussen (2006), green roofs appear to retain or delay water up to a certain precipitation rate but that once field capacity of the medium has been reached, the hydrograph for a green roof is similar to that of a standard non-vegetated roof.

Literature evidence for the thermal performance of green roofs suggests that these structures can provide a reduction in roof temperature and heat flux into buildings during the summer months. Fioretti et al., (2010) provide evidence of an intensive green roof maintaining a relatively constant and reduced temperature compared to that of a traditional roof at their test site in Ancona, Italy. Average temperature reduction under the green roof ranged between 2.45^{o}C and 7.26^{o}C over the summer period. Niachou et al., (2001) reported that there was not a significant difference between surface temperatures of green roofs and insulated buildings, but that the interior room temperature of similarly insulated buildings was 2^{o}C lower in a building with a green roof than one with a conventional roof. They also found that during a 4 day period with no occupancy the green roof building's interior temperature exceeded 30^{o}C 15% of the time, whereas the one without a green roof exceeded 30^{o}C 68% of the time. And Lazzarin et al., (2005) reported a 60% reduction in thermal gain of a room underlying a greenroof as opposed to one within a traditionally roofed building.

It is postulated that this reduction in temperature is achieved by both shielding of the underlying soil from direct solar radiation by the foliage, and by the latent heat flux associated with evapotranspirational losses.

Winter performance of green roofs is less clear cut, with the same Lazzarin study finding that in the winter a green roof lost slightly more heat to the environment than the conventional roof. However, Castleton et al. (2010). after Liu and Minor (2005) report an average reduction in heat loss through a Toronto green roof in winter of 10-30%. Theodosiou (2003) states that only a deep media construction can offer an insulation effect during winter without insulation.

Both Lazzarin et al. (2005) and Sailor et al. (2008) point out the importance of moisture content on the thermal performance of the green roof, but few studies appear to attempt to simultaneously model the hydraulic and thermal behaviour of a green roof by matching observed seepage and temperature to computed values. The purpose of this study is to investigate whether it is possible to accurately model the

thermal and hydrological behaviour of a green roof simultaneously, and to investigate the application of the validated model to a range of green roof scenarios.

2 Experimental Site Characterisation

The University of Birmingham test array is located on the 5-floor of the Watson building on the main University of Birmingham campus, Birmingham, UK (52´´27´01.54´´N, 1´´55´43.41´´W), and was completed on 12/3/2007 (Adams *et al.* 2007). The university test site comprises 35, 3 m^2 brown roof mesocosms. There are five replicates of each of seven different mixes of recycled aggregate seeded with a wildflower seed mix. Aggregates used in the study were sourced locally, and were considered 'waste' aggregates in the UK before the recent establishment of landfill taxes and aggregate levies. The mesocosms were established in May 2007 and the development of plant and invertebrate assemblages on the plots has been, and continues to be, intensively studied. In order to explore possible trade-offs between the ecological and hydrological benefits of the different substrate types, the hydrological performance was measured for two of the aggregate mixes (Bates *et al.*, 2009) and has provided the data for the current study.

Mesocosms consist of a plywood deck (2.44 x 1.22m) with timber curbs at all sides and a 50mm drainage outlet. A sheet of polyester reinforced PVC is used as a waterproof and root resistant layer, above which sits a composite drainage-reservoir board and fleece layer (Figure 1). The drainage-reservoir board allows free drainage of the substrate and provides a temporary store of water. The fleece layer limits the amount of fine sediment that washes through the mesocosms.

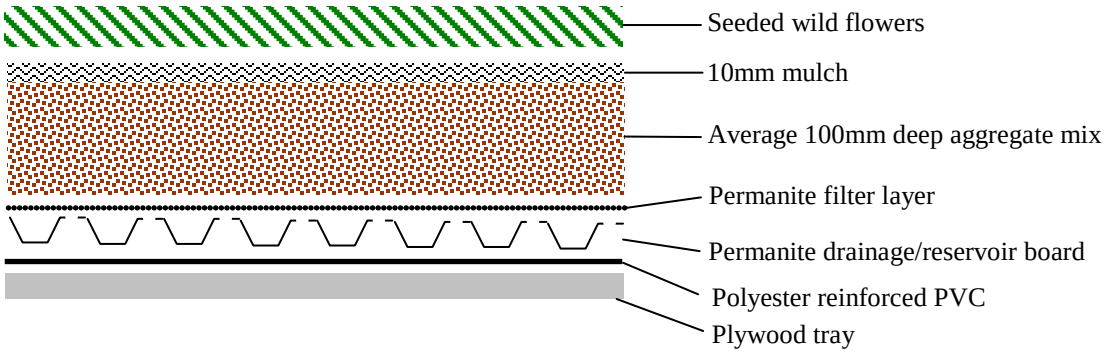

Figure 2.1 Brown roof tray design used in this investigation

Bengtsson (2005) has shown that altering the size of experimental green roof plots does not alter the hydrological response of the plots as the response is controlled by vertical, rather than horizontal flow characteristics. Therefore the relatively small size of the experimental mesocosms is sufficient for the purposes of the investigation.

The substrate layer of each mesocosm was composed of 100mm of either crushed brick aggregate or demolition aggregate (predominantly concrete) with 10 mm of sandy loam mulch, and was seeded with the same seed density (~1.6g per m^2) and mix of wild flowers comprising 24 species present on local brownfield sites, together with species known to thrive on brown roofs.

3 Monitoring

The hydrological performance of the mesocosms was monitored throughout the study period. Combined run-off from the five replicates of the study treatment for each of the two substrates, demolition and brick, was measured using a small V-notch weir, calibrated in situ using known flows from a constant head tank. The depth of the water behind the weir was measured using an ultrasonic transducer and these data were used to calculate run-off. Soil moisture and temperature probes were also installed in one replicate of the treatment to provide information on soil moisture and soil temperature at the surface and at 5cm depth below surface in the substrate. The local microclimate was measured using a weather station and pyranometer to give readings of temperature, rainfall, wind speed, wind direction, relative humidity and solar radiation. This information has been used to monitor the amount of water entering the roof mesocosms and to explore local weather effects on evapotranspiration rates, soil moisture content and soil temperature. All data were measured continuously and logged every five minutes.

4 Methods

4.1 The Modelling Software

The modelling software adopted for the study is FAT3D-UNSAT-HEAT (Law and Mackay, 2010). This finite difference computer program solves Richard's equation in three dimensions for saturated/unsaturated fluid migration in addition to contaminant and thermal energy transport. The model cannot simulate vapour transport within a medium. The model simulates radiative, convective and sensible heat fluxes at external surfaces and can model precipitation and evaporative and transpiration processes consistent with the energy fluxes. Convective heat fluxes to the atmosphere are calculated using a first order linear approximation [$J = C_t(T_{soil} - T_{atmosphere})$]. Evaporation employs the concept of Potential Evaporation to determine actual evapotranspiration. Actual evaporation is determined as a predefined function of moisture content. While not required for the present study, the model can simulate water freezing within the medium. A range of boundary conditions can be employed for drainage and seepage at the boundaries of a medium. Material properties can be spatially variable, although anisotropy is assumed to be aligned with the model grid axes for unsaturated flow simulations.

Soil moisture characteristics are characterised using the Van Genuchten equations (Allen *et al.*, 1998). Local thermal equilibrium between the rock grains and water is assumed. Material properties are assigned using user-defined material types.

Timestepping is automatically determined by FAT3D-HEAT-UNSAT. All time variant data are assumed to be piece-wise constant between input observed value values.

Given the shape of the mesocosms, modelling adopted one dimensional vertical flow only with a seepage boundary condition applied to the base of the mesocosm and a combined precipitation, evaporation boundary condition applied to the top surface boundary.

5 Data Management

The model requires flow, transport and thermal property values for all materials at all points within the model in order to solve the heat and mass flow equations. These can be broken down into two groups, those which can be directly measured (or calculated from parent data) and those that must be initially estimated and then improved during subsequent simulations. The time variant data (T, P, ET, E) were input in a list format which FAT3D-UNSAT-HEAT was able to read and incorporate into its calculations for each timestep. Air temperature and precipitation were directly measured, but the energy input per unit volume of material and the potential evapotranspiration during each timestep were derived from related raw data. Energy input into the brown roof system was calculated as:

measured solar radiation x (1-albedo) (1)

and reported in KJ/m3/day. An albedo value of 0.4 was selected based upon the surface reflectance of the mesocosms, consistent with Sailor et al.(2008). Potential evapotranspiration was calculated using the Penman-Monteith equation as advocated by the FAO (Allen *et al.*, 1998).

The Penman-Monteith equation is as follows:

$$ET_0 = \frac{0.408\Delta(Rn - G) + \gamma \frac{900}{T + 273} u_2(e_s - e_a)}{\Delta + \gamma(1+0.34u_2)} \quad (2)$$

Where:

ET_0 – reference evapotranspiration [mm/day]
Rn – net radiation at the crop surface [MJ/m2/day]
G – Soil heat flux density [MJ/m2/day]
T – mean daily air temperature at 2m height [oC]
u_2 – Wind speed at 2m height [m/s]

e_s – Saturation vapour pressure [kPa]
e_a – Actual vapour pressure [kPa]
$e_s - e_a$ – Saturation vapour pressure deficit [kPa]
Δ – Slope vapour pressure curve [kPa/oC]
γ – Psychrometric constant [kPa/oc]

The input parameters were calculated as averages over each 5 minute timestep, (with the exception of the psychrometric constant, which was fixed) but were deployed within the Penman-Monteith equation in the units as set out in Eq(2). The average ET values were found to be within the expected range for each month of the 15 month period that data existed (Cuthbert, Per Comms, 2010) and so the ET_0 values were assumed to be an acceptable estimate of the potential evapotranspiration occurring from the brown roof. For detailed of the method of transformation of the meteorological variable to derive the model input parameters consult Allen *et al.* (1998).

6 Calibration / Validation Strategy

The hydraulic parameters required by the FAT3D-UNSAT-HEAT software are as follows: (K – daturated hydraulic conductivity, θs – saturated moisture content, θr – residual moisture content, α – van Genuchten scaling parameter, n – van Genuchten shape parameter, C – seepage conductance, WP – wilting point moisture content, RC – root constant moisture content, F – actual evaporation reduction factor for moisture content less than RC). The θs and θr values employed were the USGS standard characteristics for a loamy sand, and the remaining parameters (K, α, n, C, WP, RC, F) were refined during the calibration procedure. Heat transfer parameters (k – thermal conductivity, Cp – thermal capacity, Ct –thermal convective conductance between soil and the atmosphere) were also varied during the calibration phase to achieve best fit to the observed temperature data.

The calibration procedure involved matching the seepage hydrographs and the daily temperature oscillations for the observed and modelled data for a single observation period, with particular attention being paid to harmonizing peak seepage rate and maximum and minimum temperature, along with the timing of these peaks relative to the recorded data points. Two 10 day periods and one 20 day period were selected from the parent data set and employed for calibration and validation of the model. These periods were 14 – 23 July 2007, 30 July – 18 August 2008 and 28 August to 6 September 2008. Owing to suspected inaccuracies within the recorded data for winter/spring rainfall vs seepage events, the calibration periods were drawn from a reduced data set clustered around summer periods.

Statistical analysis of the final output results from FAT3D-UNSAT-HEAT was conducted using Microsoft Excel and included linear regression, analysis of variance (ANOVA) and calculation of relative percentage differences (RPD), to ascertain the goodness of fit between the observed and predicted values for seepage and temperature. These analyses involved parametric tests which assume normality of

data. As the sample size was large for the calibration and validation events ($2882 < n < 5761$) the data were assumed to fit to a normal distribution and the use of such parametric tests were justified (Statsoft.com).

Validation was then undertaken using observations omitted from the calibration data sets to determine the adequacy of the final model of the brown roof mesocosms.

Graphical results from the different Calibration and Validation exercises are fully described in Appendix 1.

7 Results

7.1 Final model parameters

Table 7.1 identifies the final calibrated variables derived from the calibration validation processes.

Parameter	Symbol	Value	Units
Hydraulic conductivity	K	10	m/d
Saturated moisture content	θs	0.41	-
Residual moisture content	θr	0.057	-
Alpha	α	10	cm^{-1}
n	n	2	-
Thermal conductivity	k	250	KJ/m/d/^oC
Heat capacity	Cp	2000	KJ/m^3/^oC
Seepage conductance	C	2.5	m^2/d
Thermal conductance	Ct	2000	?
Root constant	RC	0.1	-
Wilt point	WP	0.08	-
F-reduction	F	0.1	-
Precipitation temp		10	^oC

Table 7.1 Final calibrated/validated Aggregate and Boundary property values

Saturated and residual moisture contents were taken from the USGS Rosetta database values for a loamy sand. The van Genuchten α and n values were varied during calibration given the unusual nature of the aggregates sued as the brown roof substrate. The final values lie between the expected values for a sand and a sandstone. The result can be explained by the coarseness of the crushed aggregates with grain size of typically 20 to 40 mm diameter and embedded in fine crushed materials. Thermal conductivity was concluded to be 250 KJ/m/d/^oC, which is consistent with the conductivity values associated with average soil minerals, and slightly higher than the reported thermal conductivity value of brick – 112.32 KJ/m/d/^oC (Stonestrom and Constantz, 2003). Heat capacity was also in the range reported for soil organic matter and minerals, but was once again closer to values

associated with soil than those reported for brick, which made up the bulk of the drainage layer of the green roof. This is in contrast to the findings of Sailor et al., (2008) who state that literature values of naturally occurring soils are not representative of ecoroof properties. The difference here could be due in part to the addition of a growth substrate to the surface of the substrate and to the presence of a high percentage of fines that fill the pore spaces of the large aggregates.

Thermal conductance in the temperature boundary condition was set to 2000 $kJ/m^2/^oC/day$ which was at the very upper limit of what we considered to be a reasonable value based on an analysis of the apparent thermal conduction values used in the Penman Monteith equations that quantify the mean impact of wind turbulence on the energy and evaporative fluxes at a land surface in the UK. Values lower than this resulted in the model storing too much heat and producing accentuated peaks when compared to the observed temperature data.

The model proved to be relatively insensitive to evaporative parameters, presumably because the water content never dropped low enough within the green roof for these factors to come into play. The Root constant value employed is similar to that measured by Hilten et al. (2008) who recorded field capacity and wilt point of 0.11 and 0.08 respectively. Bengtsson et al., (2004) measured wilt point to be around 0.15 for a 3cm deep substrate layer on top of 1cm of crushed stone aggregate.

The factor that exerted most control on the model was the conductance term of the seepage boundary condition. This controls the rate at which water can leave through the bottom of the modelled green roof. Reducing this conductance term was the only way that a reasonable fit to the observed hydrograph could be achieved within the model. This low conductivity is hard to explain given the nature of the coarse brick drainage layer, but most likely represents the sealing of the thin geotextile permanite filter layer, designed to prevent fines leaving the green roof plot within the seepage volume. This material and the material deposited on top of it forms a low permeability layer sufficient to justify the use of a conductance term as low as the 2.5 m^2/d employed in this simulation. Indeed, Simmons et al., (2008) found evidence in their investigation into 6 types of green roof that those with a high retention cup capacity and low drainage hole area exhibited the highest retention overall.

7.2 Results

7.2.1 Seepage performance

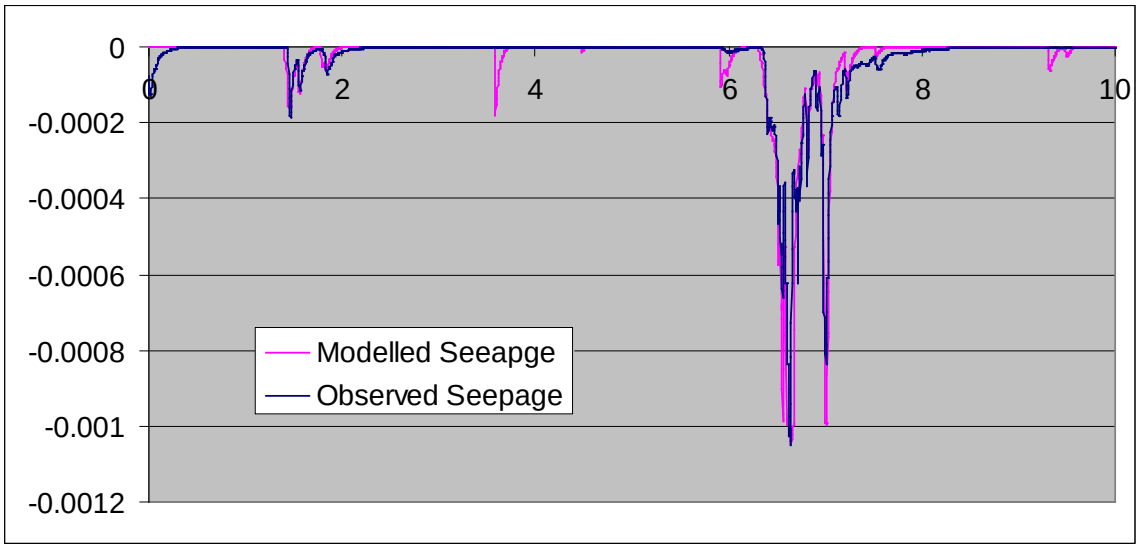

Figure 7.1 Comparison of modelled to observed seepage – Calibration period A

The hydrographs of the modelled and observed seepage during the calibration A period are illustrated in Figure 7.1 show a very good level of agreement. There is an anomalous peak at day 3.5, which could not be removed during the calibration process, but otherwise the timing and peak magnitude of the modelled seepage match the observed data very well. Indeed, the relative percentage difference (RPD) between the observed and modelled peaks is 11.8% for the peak at day 1.4 and just 0.7% for the peak at day 6.6. Peak timings were also well matched with no delay for the first peak and just a 5 minute difference between observed and modelled peak seepage at day 6.6. There was again no difference in timing of the observed and modelled peaks for day 7, however, this point also demonstrated an overestimate of the seepage by the model of 19%.

The observed vs modelled seepage graph (Figure 7.1) shows that while the statistical performance is good, there is an indication that the model tends to over-predict for the intermediate values, and under-predicts for the very largest seepage rates.

For the Validation A period (Figure 7.2), the model once again replicates the observed seepage hydrograph with a good accuracy. RPD for the peaks range from 10.4% to 22.2%, with most time lags between the measured and observed peaks being either 0 or 5 minutes. The greatest time lag is 70 minutes between the same modelled and observed peak, which can be seen to be the peak at day 9.6. There is one outlying RPD value for seepage of 47%, corresponding to day 6.7. This can be explained by noting that the model has a higher antecedent moisture content than the physical green roof at the beginning of this seepage event.

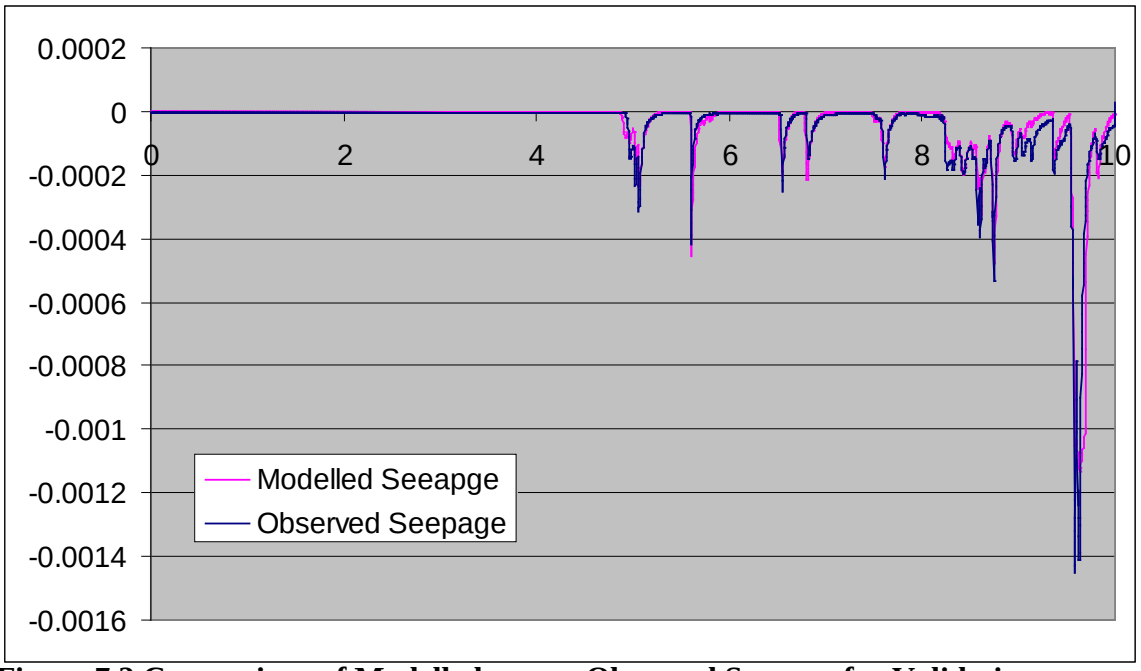

Figure 7.2 Comparison of Modelled versus Observed Seepage for Validation Period A

The modelled versus observed seepage graph yields an R^2 value of 86%, and visually the fit is good, with a cluster around the 45^o line at the lower seepage rates. However, there is an apparent deviation from the 1:1 relationship at intermediate seepage rates, evidently caused by the model over-predicting the equivalent seepage value. This appears to be produced by one single poorly replicated seepage event over the entire 10 day period, the peak at 9.6 days. It would appear that the delay of 70 minutes between the observed and modelled peak is maintained throughout the descending limb of the hydrograph and therefore produces the relatively constant horizontal line of points in Figure 7.3. This then rapidly decays away as the next precipitation event begins. Removing the points after 9.5 days that largely comprise this single, large and relatively poorly replicated seepage event, yields a modelled versus observed graph as demonstrated in Figure 7.4 with a correspondingly improved R^2 value of 88.4%.

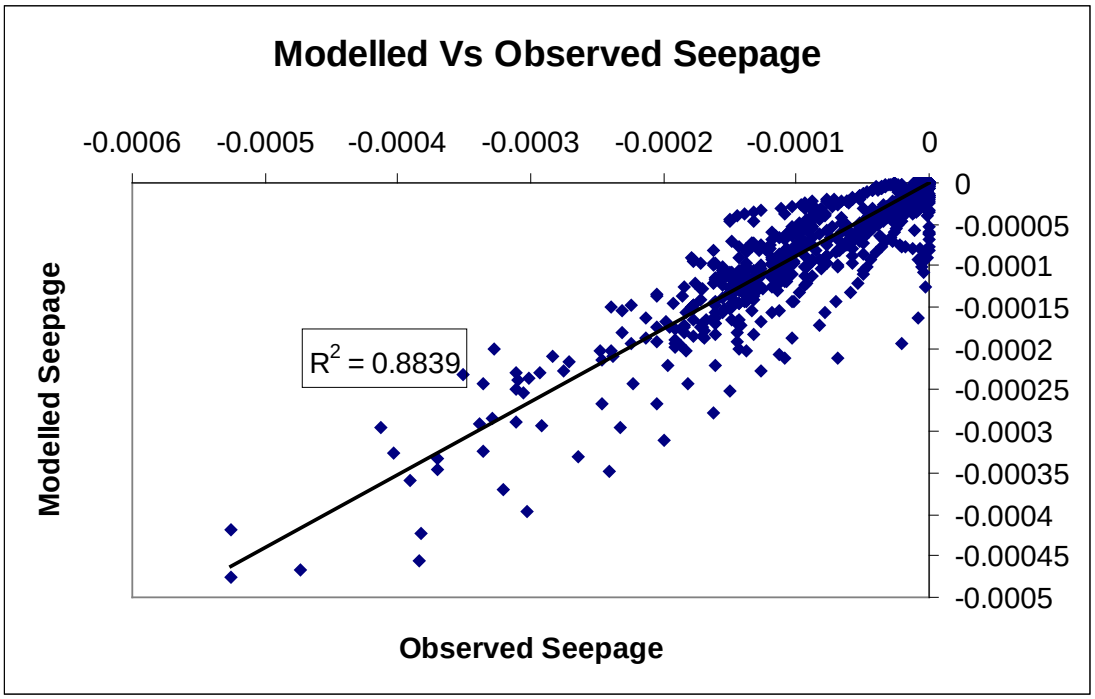

Figure 7.3 Cross plot of modelled versus observed seepage rates

The final validation period was 20 days in duration, and yielded a somewhat reduced goodness of fit value of R^2 = 67.8%. RPD between observed and modelled peaks ranged from 1.3% to 91.8%, with the majority of peaks yielding relative percentage differences of 33% or less. However, it was also noted that the agreement between modelled and observed seepage between day 13 and 15 was less impressive than had been recorded for the other calibration periods, with RPDs of 91.8%, 41.6% and 70.1% recorded over this phase. Timing of the peaks shows a closer alignment between the observed and modelled data, with the majority of lags <15 minutes. However, one peak demonstrates a lag of 95 minutes during the day 13 – day 15 period, and there is another instance at day 19 where the time between observed and modelled peak is over 6 hours. Overall, the timing of the peaks show adequate alignment. A summary of the agreement between the observed and modelled peaks is shown in Table 7.2

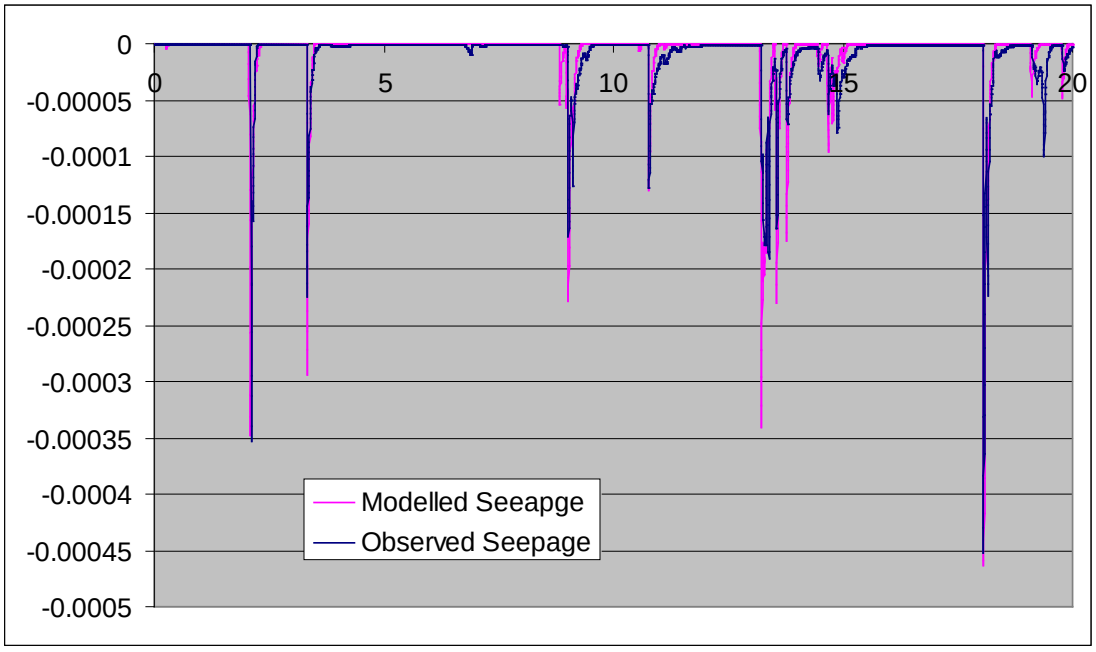

Figure 7.4 Observed versus Modelled Seepage - Validation Period B

From an analysis of the observation data for the whole period for which data were available (15 months), the total retention appears to be highest during the summer periods, with 38% and 58% retention recorded for June – September and April – July respectively. Winter retention rates are closer to 20 -25% and so the data are broadly in agreement with other studies that have shown how the observed green roof performance is dictated by climatic conditions and that during the winter months, the green roofs ability to mitigate stormwater runoff is reduced relative to their performance in summer (Spolek, 2008; Bengtsson, 2005). The final average retention value for the 15 months is 37% and comes out quite close to the value reported by Spolek (2008) who took an average value from 3 years of data recorded in Portland, Oregon, USA. Many other papers that report higher average retention are based on data recorded from short periods of time or summer periods which will potentially skew the predicted runoff mitigation performance of a green roof . Of course, this point depends on the purpose for which the statistic is employed. In practice, it would appear to be logical to define retention values on a seasonal basis. This would reflect the potentially different applications to which these data could be applied e.g. stream/river regulation or stormwater mitigation.

Essentially, seepage lag (ie the time from rainfall to onset of seepage) is dependent on the antecedent soil moisture conditions and rainfall intensity, rather than time to preceding seepage event. It is the finite storage volume of the roof, and the speed with which this is restored or filled up after or before a rainfall event respectively that determines the seepage response of a green roof. This observation confirms the previous work of other authors.

7.2.2 Thermal performance

The model replicates the thermal performance of the green roof very well, with an R^2 value of 91.4% for the calibration period. As can be seen visually from, Figure 7.5, the agreement between the magnitude of the temperature, and particularly the timing of the peaks and troughs, is striking.

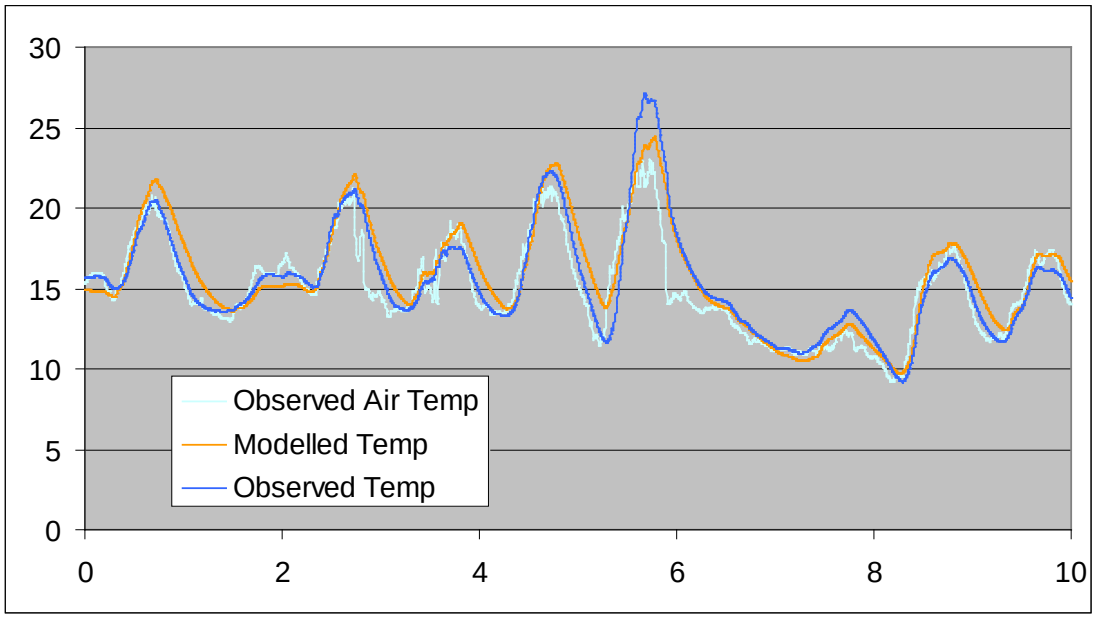

Figure 7.5 Modelled and Observed Roof temperatures for Calibration Period A

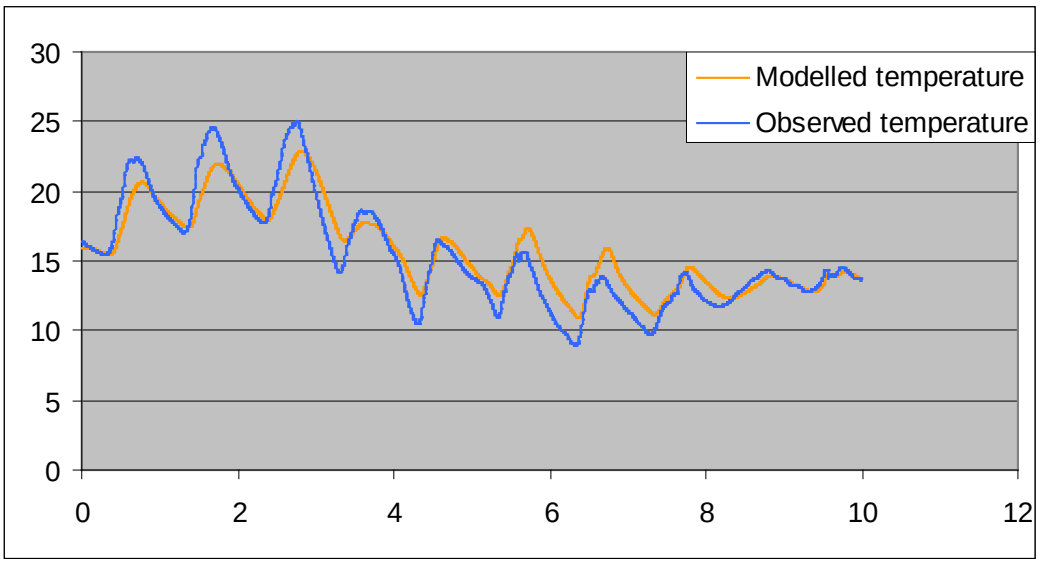

Figure 7.6 Comparison of Modelled versus Observed Temperatures for Validation Period A.

The lag between observed and modelled peak temperature is a maximum of 95 minutes, with the majority of peaks being less than 15 minutes different from the observed data. The maximum difference between recorded and modelled peak temperatures, as a ratio of the total temperature range, is 13%, and the minimum just 2.3%. Analysis of the difference between minimum temperatures shows a similar degree of agreement between modelled and observed, with the maximum variation in temperature measured at 12.1%, with a minimum difference of 0.08%.

For the "Validation A" period, Figure 7.6, visually the fit looks less impressive, with an apparent trend of model under-prediction during the early phase of the graph, and a tendency to over-predict during the later phase. Despite this, statistical analysis of the data yielded an R^2 value of 93.96%, which would indicate a high level of agreement between the observed and modelled temperatures. Maximum RPD between the peak temperatures is 16.4% with a minimum of 1.39%. Low temperatures over the period had a maximum RPD of 19.98% and a minimum of 0.36%.

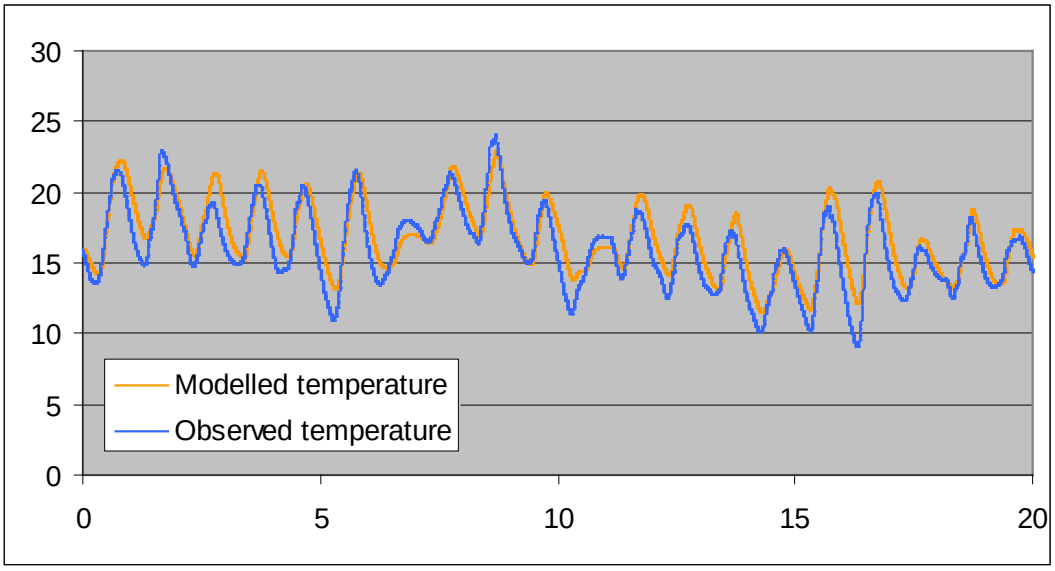

Figure 7.7 Comparison of the Modelled versus Observed response for Validation Period A2.

The 20 day validation period (A2), Figure 7.7, gives a visual impression of high correlation, although statistically the goodness of fit R^2 value is 89.9%, lower than that for the other calibration/validation periods. Visual inspection of the graph does appear to indicate a proclivity of the model to over-predict temperature values. However, the peak RPD values are clustered around the 0-5% range, with only a few peaks nearing the maximum RPD of 11.62% as witnessed on day 3. Minimum RPD for peak temperature was 0.12%.

The median average RPD for "Validation 2" is the smallest of all three calibration/validation periods (4.44%), despite its lower R^2 value, and indicates that it has a higher proportion of its peak data points correlating closely to the observed data value. Its lower R^2 value may indicate that the observed and modelled data deviate from each other slightly more in between peaks. The model is slightly worse at

replicating the low temperatures during this period, as demonstrated by the maximum RPD of 33.28%. However, it still generates a median average of 6.48% RPD, indicating that high values such as differences of 33.28% are outliers and that the model is on the whole replicating the temperature data to an acceptable degree of accuracy.

7.2.3 Predictive application of the model

The 10 day period (Period A) used for calibration was employed in a predictive capacity to investigate the effect increasing the depth of the media would have on the thermal and hydraulic behaviour of the green roof. All model parameters were maintained from the final calibrated model, and the measured and derived meteorological input data were also unaltered. Only the media depth was changed, increased by 0.12m each time from the original 0.12m to 0.24m, 0.36m and finally 0.48m. Seepage hydrographs and predicted temperatures at the midpoint of each profile were compared to investigate the effect that increase in media depth would have upon the green roofs performance. The findings are displayed in Figure 7.8

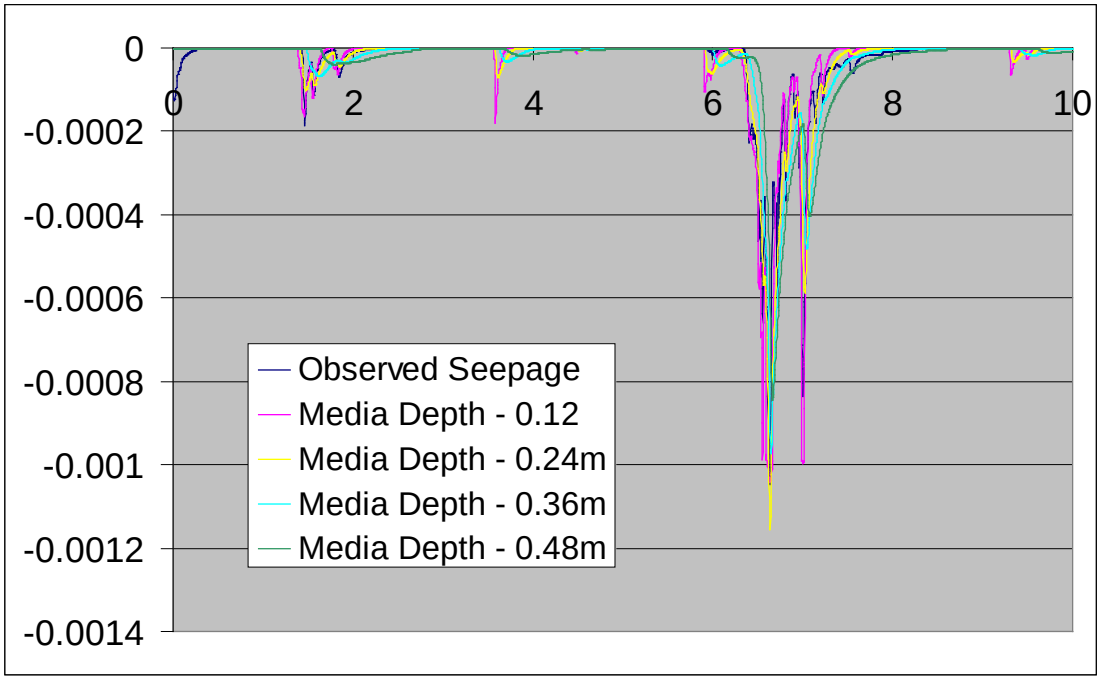

Figure 7.8 Impact of increasing depth of substrate on the seepage performance of the Brown roofs

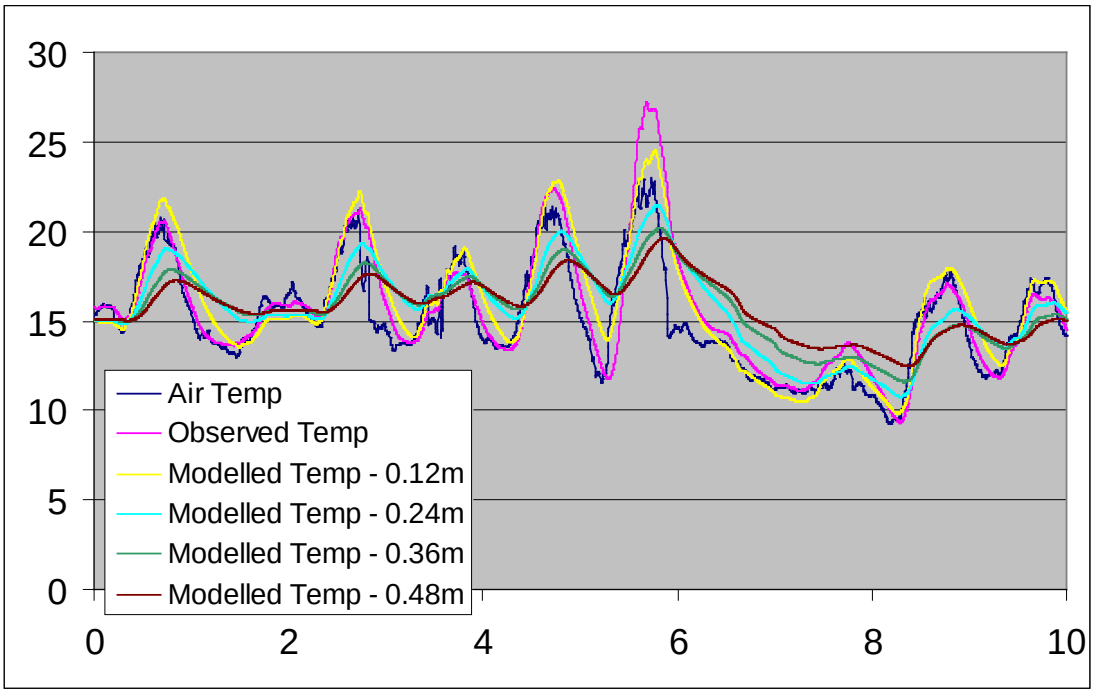

Figure 7.9 Impact of increasing thickness of substrate on the thermal performance of brown roofs.

As Figure 7.9 shows, temperature appears to moderated by the increasing depth, with peak temperatures reduced compared with the observed and original 0.12m deep green roof. Also, it is apparent that low temperatures are increased, resulting in a temperature signal that becomes more stable as the depth increases. This is borne out by an analysis of the data values which indicate that the maximum temperature for the 0.12m deep media over the 10 day calibration period is 27.2^{o}C, which falls to 19.5^{o}C for the 0.48m medium. Minimum temperatures are increased from 9.3^{o}C to 12.3^{o}C as again media thickness increases from 0.12m to 0.48m, whereas the average temperature is maintained relatively constant, ranging from 15.54^{o}C to 15.75^{o}C over the entire range of media depths. These results suggest that as the depth of media increases the high and low temperatures at the surface propagate less and less to depth within the media profile. Therefore, minimum temperatures increase, and maximum temperatures decrease, as both tend toward the average value of approximately 15^{o}C.

Figure 7.8 also indicates that increasing media depth appears to delay and reduce the peak seepage rates relative to the observed data. For the first peak at around day 2 into the observation period, doubling media depth to 0.24m resulted in a 38.8% reduction in maximum seepage rate. A further increase to a 0.36m deep media resulted in a 59% drop in peak seepage rate, and the final media depth of 0.48m resulted in a 77.5% decline in the peak seepage rate. However, the high proportion of peak signal attenuation was not witnessed for all seepage events. The seepage event at around day 6 saw a maximum reduction of 19% in the peak seepage, and actually saw an increase compared to the original media thickness when the media depth was doubled to 0.24m. This is difficult to explain given that the model assumes uniform properties with depth. One explanation might be the non-linear behaviour of the flows in response to changing moisture contents that allow retention of a higher depth

of saturation at the base of the substrate layer that can be more rapidly mobilised when moisture is added from drainage from the surface.
Peak timing was delayed by increasing media depth, although again this effect varied considerably. For the day 2 peak, doubling media depth to 0.24m provided just a 20 minute delay in peak seepage rate. However, 0.36m of green roof medium delayed the peak runoff rate by almost 4 hours, and increasing to 0.48m of media doubled this lag to 8 hours. For the larger peak on day 6 though, 0.48m of media only delayed peak seepage rate by 1 hour, although this delay could still prove valuable in an integated stormwater management system.

Fioretti et al. (2010) state within their literature review that though an increased media depth does result in higher retention, the gain is not large. This is broadly in agreement with our findings, with only a 0.8%, 6.4% and 9.5% increase in the total precipitation retention witnessed by increasing the media depth to 0.48m for each of the three calibration/validation periods. What our data do indicate is the ability of increased media depth to attenuate and delay peak runoff rates, correspondingly releasing a similar runoff quantity but over a longer timescale. This supports other authors findings and could provide benefits (reduced strain on stormwater systems that are currently expected to operate beyond design capacity) if these properties were exploited as part of an integrated stormwater management plan.

To investigate the effect depth of media has on rainfall retention, and to attempt to characterize the media depth that could completely eradicate seepage from a rainfall event, the simulation was run again with the calibrated parameters but with only one artificial rainfall event occurring throughout the entire 10 day period. This was varied for each media depth, but always began at midnight on the second day (24 hours into the experiment), and was applied to a profile that would have experienced dry conditions for some time. To achieve this end a moisture content of approx 0.1 (the Root constant) was used as the initial moisture content of the media, achieved through systematic variation of the suction head applied to the model in the initial conditions. This dry profile then provided the best case scenario for predictive modelling of the retentive water capacity of the green roof and the effect media depth had upon this character. Energy input to the model, evaporative flux and precipitation temperature were all maintained from the actual measured or derived values as used within the calibration process, and in the case of the evaporative loss, could be a source of criticism of the overall accuracy of this estimate. However, as the effect of media depth was to be compared within the same model with the same conditions, it was deemed sufficiently accurate to be able to draw conclusions of the relative behaviour of this green roof with various depths.

Rainfall events were maintained at constant rates for periods of 6 hours, and the total volume was systematically altered until a minimal seepage rate was achieved (<0.5mm). This was deemed to be the precipitation volume required to induce seepage for the relevant media depth employed within the model, and was repeated for 0.12m, 0.24m, 0.36m and 0.48m deep simulations.

In contrast to the earlier small retention increase afforded by deeper media, when the precipitation input file was amended so that only one artificial rainfall event occurred

there was a marked difference in the precipitation volume that was required to induce seepage for each of the 4 media depths incorporated. This is perhaps more intuitive as a deeper medium has more void space and so has a greater volume available for storage of precipitation until seepage begins. The 0.12m media depth, a direct representation of the experimental green roof plot, required a precipitation event of 31mm at a rate of 0.124m/d over a 6 hour period before seepage was initiated. The 0.24m deep medium could accommodate 45mm of rainfall at a rate of 0.18m/d before seepage occurred. The 0.36m media stored 48mm of precipitation at a constant rate of 0.195m/d before seepage began. In the 0.48m deep media, no seepage occurred until 52.5mm of precipitation had fallen at a rate of 0.21m/day over a 6 hour period.

This could point to the fact that the period used to model the effect depth has on retention is dominated by an extreme rainfall event, which masks the increased volume deeper media green roofs can store. Or could be an accurate response of green roofs, as there is likely to be a variety of rainfall intensities, some below the threshold the green roof can accommodate and some far above what it can store, and so that, on average, 10% is the increase that can be obtained over any period of time. At any rate, the data point to the fact that the 0.12m media could store just over half as much as the 0.48m green roof before seepage would occur. It is interesting to note the relatively small increase in storage capacity achieved by increasing media depth from 0.24m to 0.36m.

8 Summary and Conclusions

The modelling study described in this report has been used to test the development of a model of the combined hydraulic and thermal response of extensive green roofs. An existing modelling package, FAT3D-UNSAT-HEAT has been used for the study. Data from the first 15 months of data collection on the experimental roof array developed at the University of Birmingham were used to test the model. The results of the calibration and validation exercises showed that the model can provide a strong representation of the behaviour of brown roofs with thin substrates. The results also show that the lower boundary condition is strongly influential in controlling seepage rates at the base of the substrate and that this will be dependent on the material used as a filter membrane as well as the fine particle content of the aggregates.

The study demonstrates that the performance of brown roofs for stormwater mitigation is not sufficient for stormwater management. However, it does demonstrate that clear attenuation of the majority of peak flows does occur both during the summer and winter periods and that this can provide some support for regulating flows into the surface water networks in the urban area. The results also show that increasing the depth of substrate provides only limited success in both reducing the total flow from the roofs and also reducing the peak flows for natural precipitation distributions. Artificial precipitation does show substantial advantages for deep substrates, but the results are largely hypothetical.

Thermal responses of the brown roofs can be modelled well using FAT3D-UNSAT-HEAT. While the results are only proven for UK conditions, the thermal response data does show the buffering capacity of a brown roof on the heat conditions at the base of the roof. It also shows that additional cooling is provided by the enhanced evaporation at the surface of the roof. For thin roofs the moisture retention would not be sufficient to strongly mitigate the heat island effect, but more work is needed on this aspect of brown roof performance. Deep substrates do provide strong buffering of the base temperature conditions and this will be beneficial in terms of the longevity of a roof and in terms of the insulation requirements for a building.

Finally, the modelling has shown that standard material property model descriptions can be employed for the quantification of fluid flow and thermal diffusion in crushed brick wastes. This indicates that it is unnecessary to construct new constitutive models of behaviour of these materials. However, the modelling does equally demonstrate that it is necessary to carry out experimental studies to determine the values of the various property coefficients to characterise any waste form that might be employed for brown roof construction.

9 References:

Allen RG, Pereira LS, Raes D, Smith M. (1998). Crop evapotranspiration - Guidelines for computing crop water requirements. Food and Agriculture Organization of the United Nations, FAO Irrigation and drainage paper 56.

Bates, A. J, Mackay, R, Donovan, R., Greswell, R. B, Sadler, J.P. (2007) SWITCH Green Roof Project: Rationale and Experimental design

Bates, A. J, Mackay, R, Greswell, R. B, Sadler, J.P. (2009) SWITCH in Birmingham, UK: experimental investigation of the ecological and hydrological performance of extensive green roofs, Reviews in Environmental Science and Biotechnology,10.1007/s11157-009-9177-8

Bengtsson L. (2005) Peak flows from thin sedum-moss roof. Nordic Hydrology. Vol. 36 No.3 269-280.

Carter TL and Rasmussen TC. (2006) Hydrologic behaviour of vegetated roofs. Journal of the American Water Resources Association 42(5): 1261-1274.

Carter T, Jackson CR. (2007) Vegetated roofs for stormwater management at multiple spatial scales. Landscape and Urban Planning 80 84-94.

Castleton HF, Stovin V, Beck SBM, Davison JB. (2010) Green roofs; building energy savings and the potential for retrofit. Energy and Buildings 42 1582-1591.

Cuthbert M. (2010).Personal communication.

Fioretti R, Palla A, Lanza LG, Principi P. (2010) Green roof energy and water related performance in the Mediterranean climate. Building and Environment 45 1890-1904.

Hilten RN, Lawrence TM, Tollner, EW. (2008) Modeling stormwater runoff from green roofs with HYDRUS-1D. Journal of Hydrology 358, 288-293.

Jain SK, Sudheer KP. (2008) Fitting of hydrologic models: A close look at the Nash-Sutcliffe index. Journal of Hydrologic Engineering. Vol 13, No. 10 981-986.

Law, R & Mackay, R (2010) Determining fracture properties by tracer and thermal testing to assess thermal breakthrough risks for ground source heating and cooling in the Chalk, QUARTERLY JOURNAL OF ENGINEERING GEOLOGY AND HYDROGEOLOGY, Vol 43, Issue 3, p269 – 278, DI 10.1144/1470-9236/08-089, ISI:000281518900002

Lazzarin RM, Castellotti, F, Busato, F. (2005) Experimental measurements and numerical modeling of a green roof. Energy and Buildings 37 1260-1267.

Liu K, Minor J. (2005) Performance evaluation of an extensive green roof, in: Greening Rooftops for Sustainable Communities. Washington, DC,.

Mackay R. (2004) FAT3D-UNSAT: a computer program for saturated–unsaturated flow in 3-dimensions. Report, School of Geography, Earth and Environmental Sciences, University of Birmingham, Birmingham, UK;

Mentens J, Raes D, Hermy M. Green roofs as a tool for solving the rainwater runoff problem in the urbanized 21st century? Landscape and Urban Planning 77 (2006) 217-226.

Niachou A, Papakonstantinou K, Santamouris M, Tsangrassoulis A, Mihalakakou G. (2001) Analysis of the green roof thermal properties and investigation of its energy performance. Energy and Buildings 33 719-729.

Palla A, Gnecco I, Lanza LG. (2009) Unsaturated 2D modelling of subsurface water flow in the coarse-granied porous matrix of a green roof. Journal of Hydrology 379 193-204.

Palomo Del Barrio E. (1998) Analysis of the green roofs cooling potential in buildings. Energy and Buildings 27 179-193.

Sailor DJ, Hutchinson D, Bokovoy, L. (2008) Thermal property measurements for ecoroof soils common in the western U.S. Energy and Buildings 40 1246-1251.

Santamouris M. (2006).Environmental design of urban buildings: an integrated approach. Earthscan;

Schroll E, Lambrinos J, Righetti T, Sandrock D. The role of vegetation in regulating stormwater runoff from green roofs in a winter rainfall climate. Ecological Engineering 37 (2011) 595-600.

She N, Pang J. () Physically based green roof model. Journal of Hydrologic Engineering Vol 15 No. 6 458-464.

Simmons MT, Gardiner B, Windhager S, Tinsley J. (2008) Green roofs are not created equal: the hydrologic and thermal performance of six different extensive green roofs and reflective and non-reflective roofs in a sub tropical climate. Urban Ecosystems 11 339-348.

Spolek G. (2008) Performance monitoring of three ecoroofs in Portland, Oregon. Urban Ecosystems 11 349-359.

Stonestrom DA, and Constantz J. (2003).Heat as a tool for studying the movement of ground water near streams, US Geological Survey Circular 1260;

Theodosiou TG. (2003) Summer period analysis of the performance of a planted roof as a passive cooling technique. Energy and Buildings 35 909-917.

Villarreal EL. Runoff detention effect of a sedum green roof. Nordic Hydrology Vol 38 No 1. 99-105.

Voyde E, Fassman E, Simcock R, Wells J. Quantifying evapotranspiration rates for New Zealand green roofs. Journal of Hydrologic Engineering Vol 15 No. 6 395-403

Websites:

Materials Data site – http://www.engineeringtoolbox.com

Food and Agricultural Organisation - http://www.fao.org/

Statististical Software Site – http://www.statsoft.com

Appendix 1

This appendix includes a range of figures illustrating the calibration and validation performance of FAT3D-UNSAT-HEAT using the data from the Brown Roof experimental array at Birmingham University.

CALIBRATION A				
	SEEPAGE		TEMPERATURE	
Calibration				
Nash-Sutcliffe Model Efficiency	E =	0.807517	E =	0.906761
Coefficient of Determination	r^2 =	0.896159	r^2 =	0.914072
Expressed as a percentage	R^2 =	89.61592	R^2 =	91.4072
Pearson's product moment correlation coefficient	r =	0.946657	r =	0.956071
Validation				
Nash-Sutcliffe Model Efficiency	E =	0.849301	E =	0.902192
Coefficient of Determination	r^2 =	0.86242	r^2 =	0.939621
Expressed as a percentage	R^2 =	86.24203	R^2 =	93.96215
Pearson's product moment correlation coefficient	r =	0.928666	r =	0.969341
Validation 2				
Nash-Sutcliffe Model Efficiency	E =	0.554637	E =	0.845965
Coefficient of Determination	r^2 =	0.678683	r^2 =	0.898737
Expressed as a percentage	R^2 =	67.86834	R^2 =	89.8737
Pearson's product moment correlation coefficient	r =	0.823822	r =	0.948017

Calibration A - Seepage

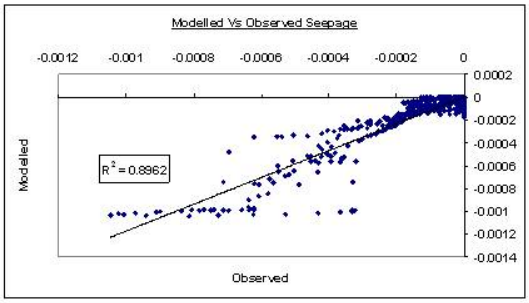

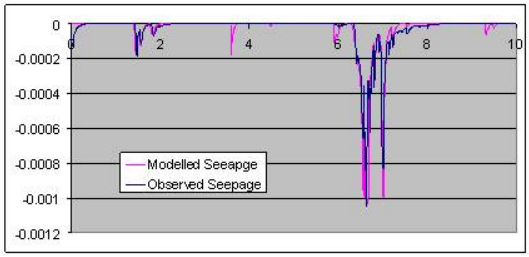

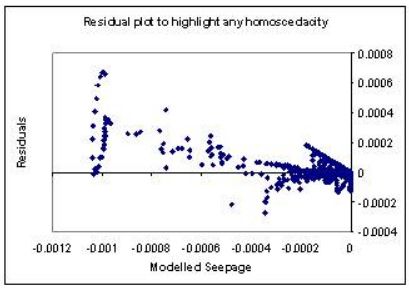

Calibration A - Temperature

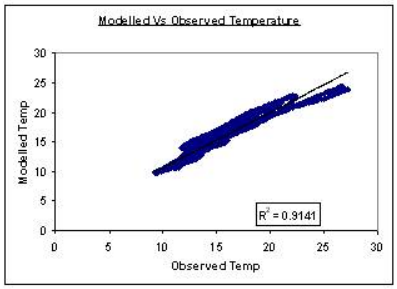

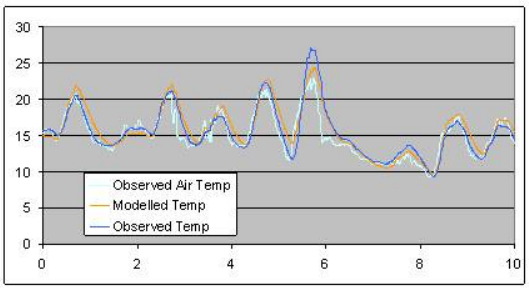

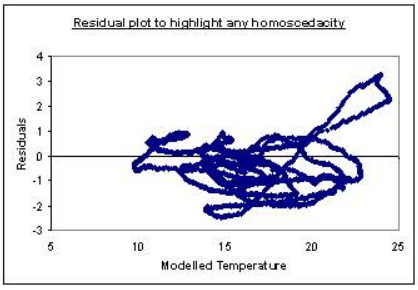

Validation A - Seepage

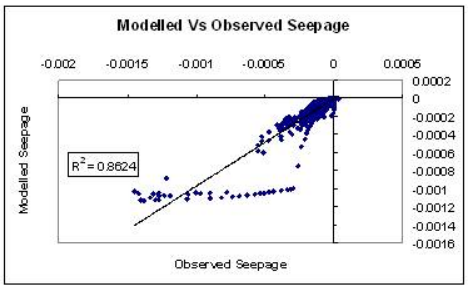

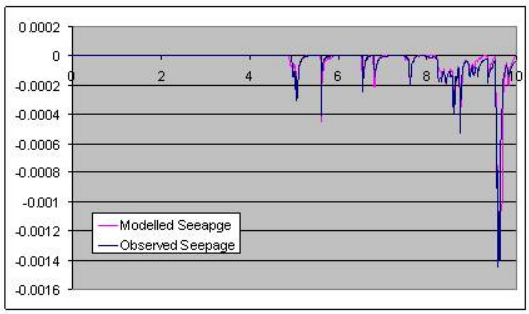

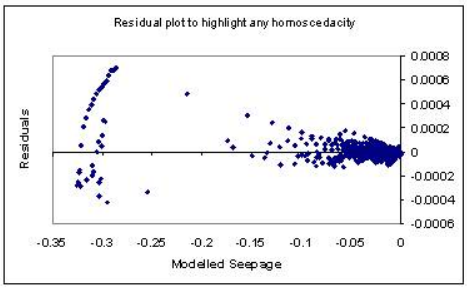

Validation A - Temperature

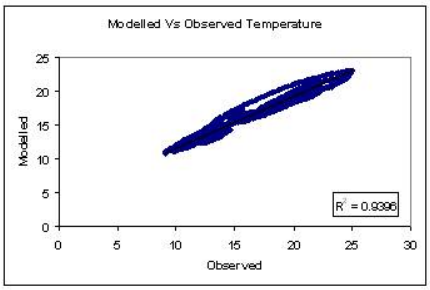

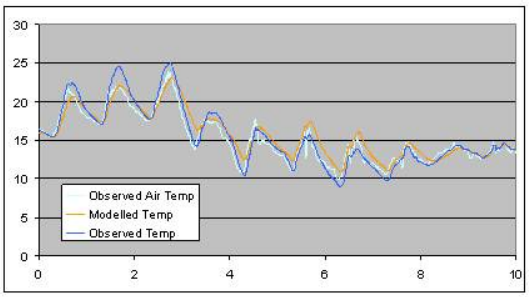

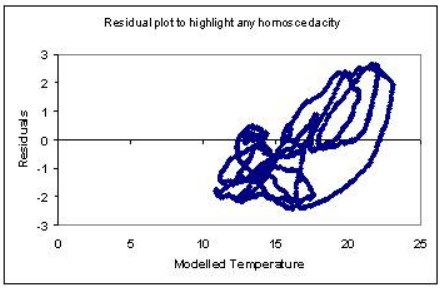

Validation A2 - Seepage

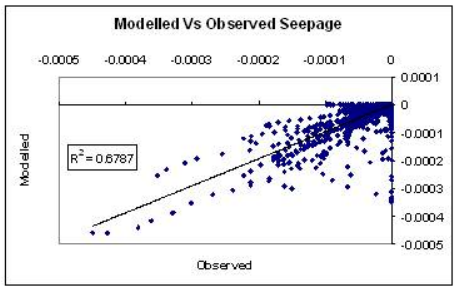

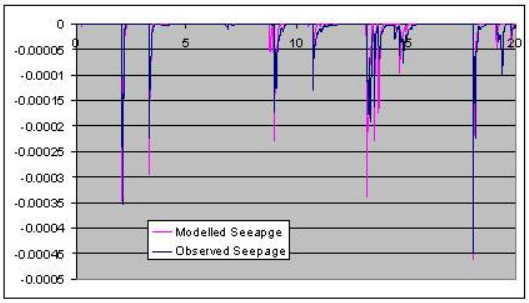

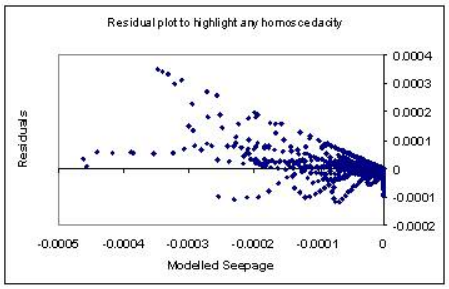

Validation A2 - Temperature

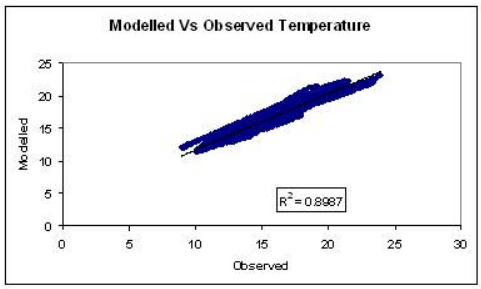

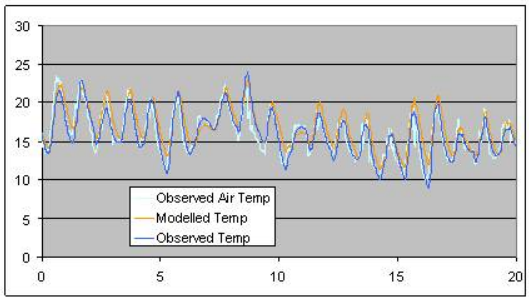

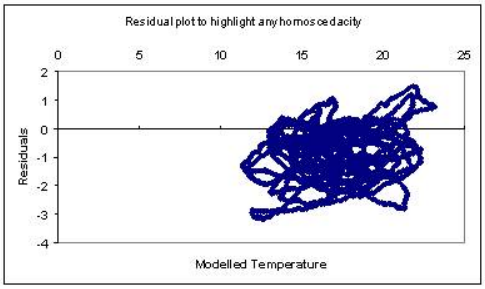

CALIBRATION/VALIDATION B

CALIBRATION B				
	SEEPAGE		TEMPERATURE	
Calibration				
Nash-Sutcliffe Model Efficiency	E =	0.774441	E =	0.926165
Coefficient of Determination	r^2 =	0.886341	r^2 =	0.926279
Expressed as a percentage	R^2 =	88.63414	R^2 =	92.62792
Pearson's product moment correlation coefficient	r =	0.941457	r =	0.962434
Validation				
Nash-Sutcliffe Model Efficiency	E =	0.827266	E =	0.951954
Coefficient of Determination	r^2 =	0.85116	r^2 =	0.978763
Expressed as a percentage	R^2 =	85.11596	R^2 =	97.87634
Pearson's product moment correlation coefficient	r =	0.922583	r =	0.989325
Validation 2				
Nash-Sutcliffe Model Efficiency	E =	0.392971	E =	0.903017
Coefficient of Determination	r^2 =	0.6589	r^2 =	0.938065
Expressed as a percentage	R^2 =	65.89003	R^2 =	93.80651
Pearson's product moment correlation coefficient	r =	0.811727	r =	0.968538

Calibration B - Seepage

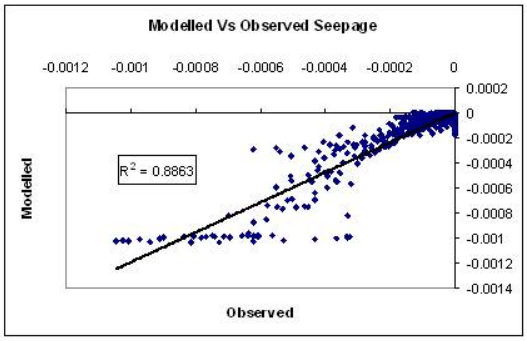

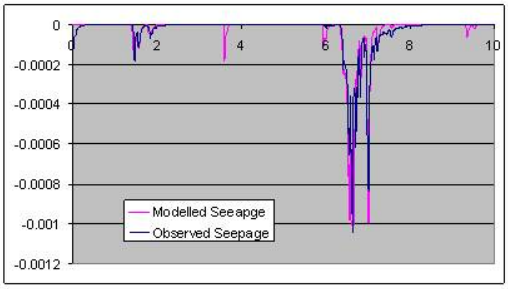

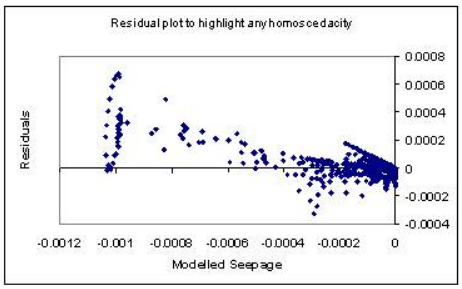

Calibration B - Temperature

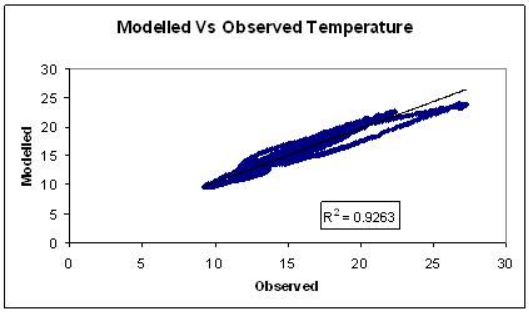

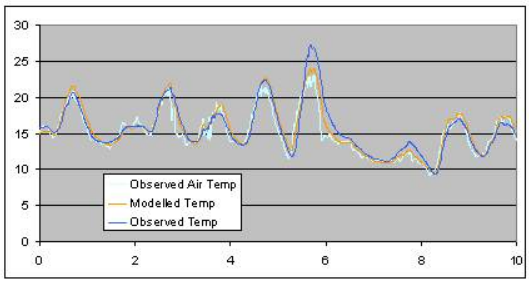

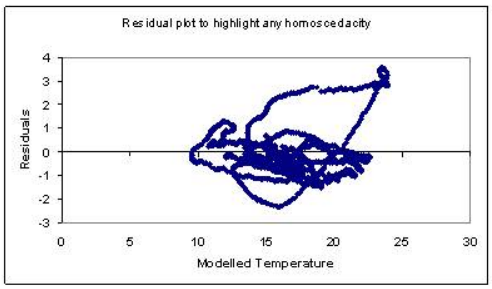

Validation B - Seepage

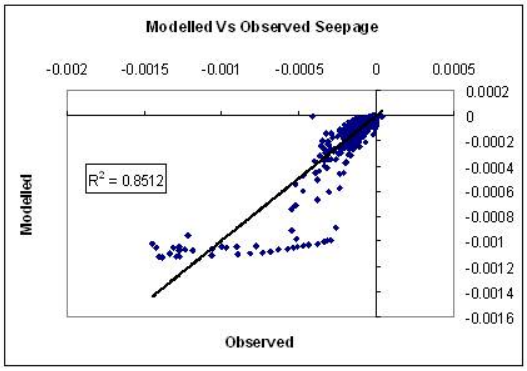

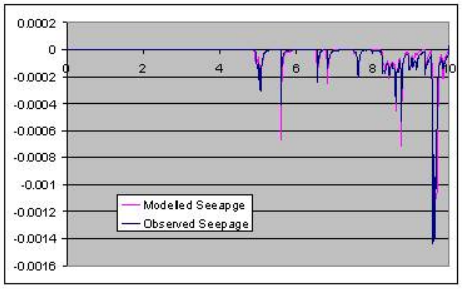

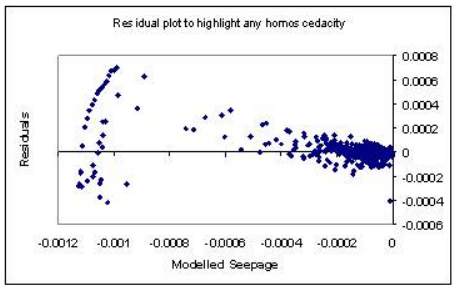

Validation B - Temperature

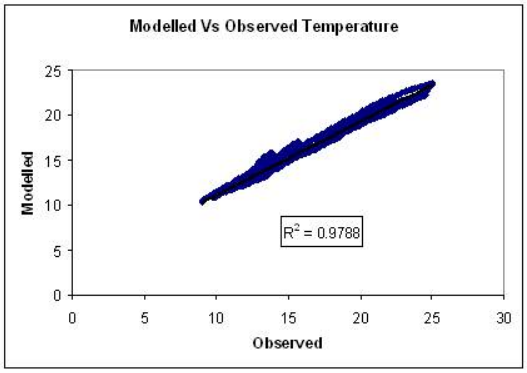

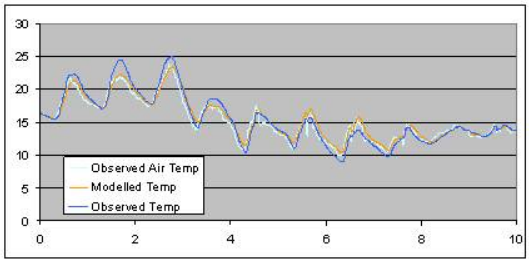

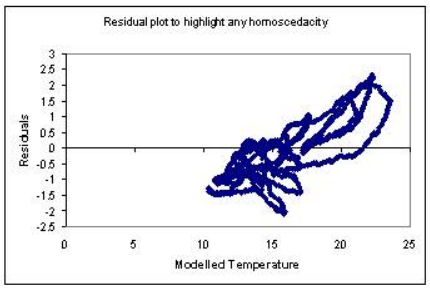

Validation B2 - Seepage

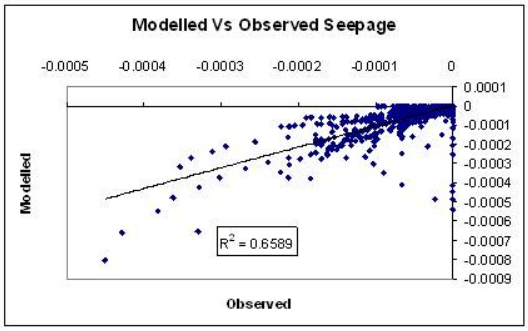

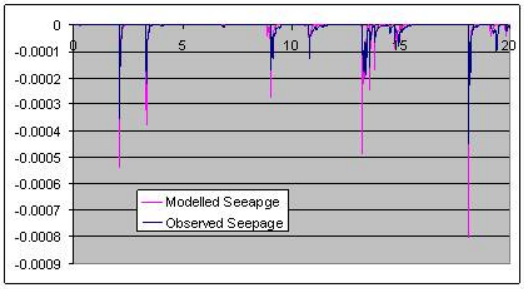

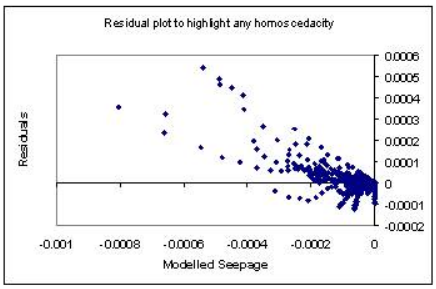

Validation B2 - Temperature

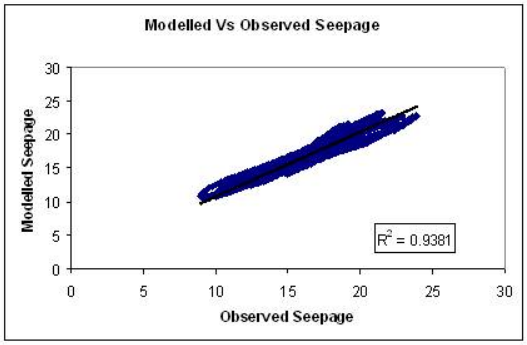

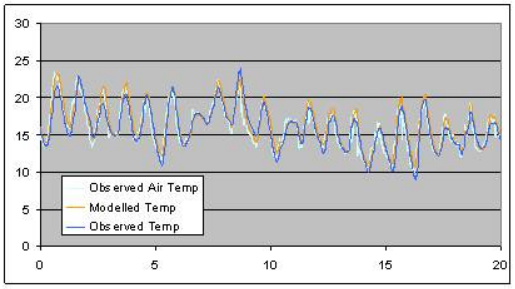

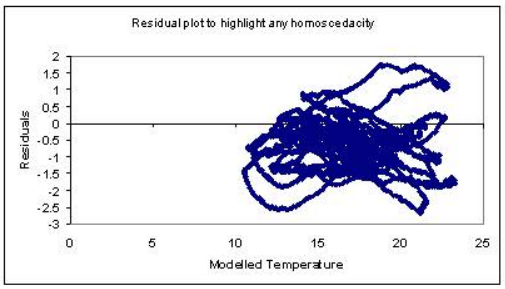

Comparisons

Validation B2 - 5000

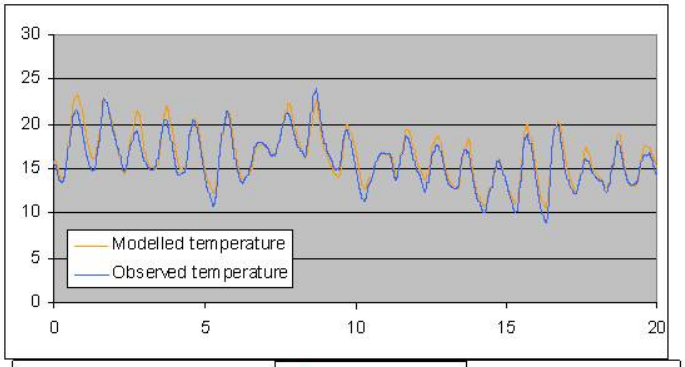

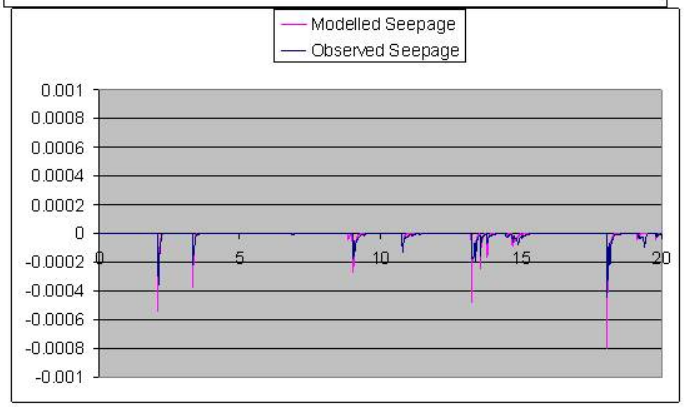

Calibration A - 2000

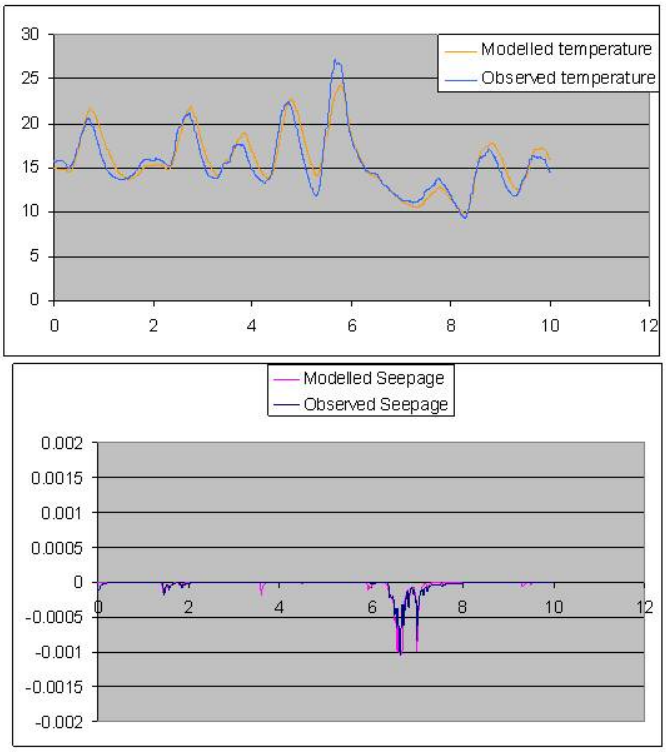

Validation A - 2000

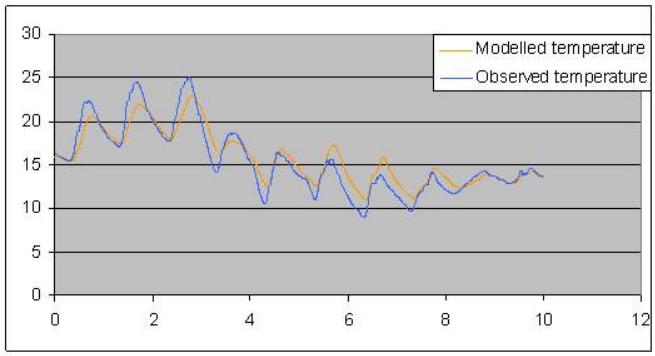

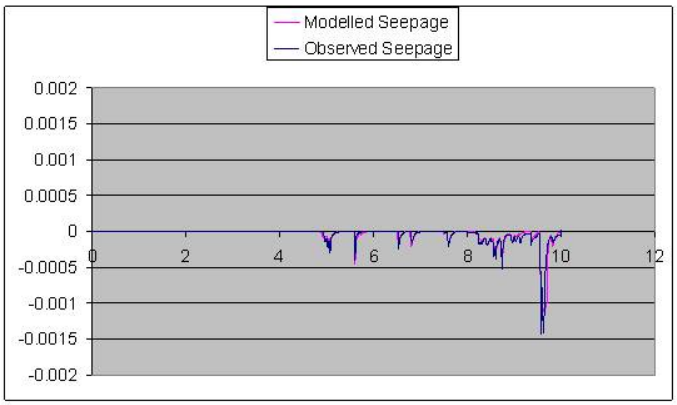

Validation A2 - 2000

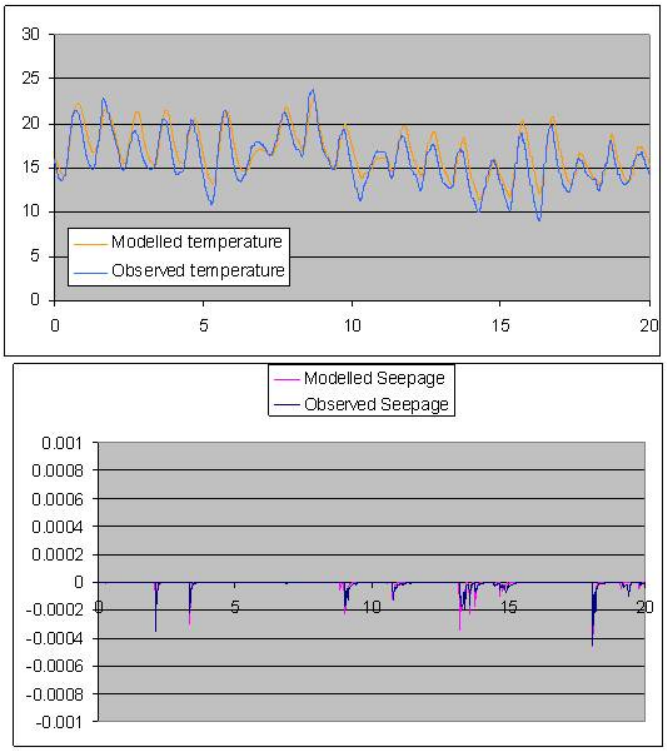

Calibration B - 5000

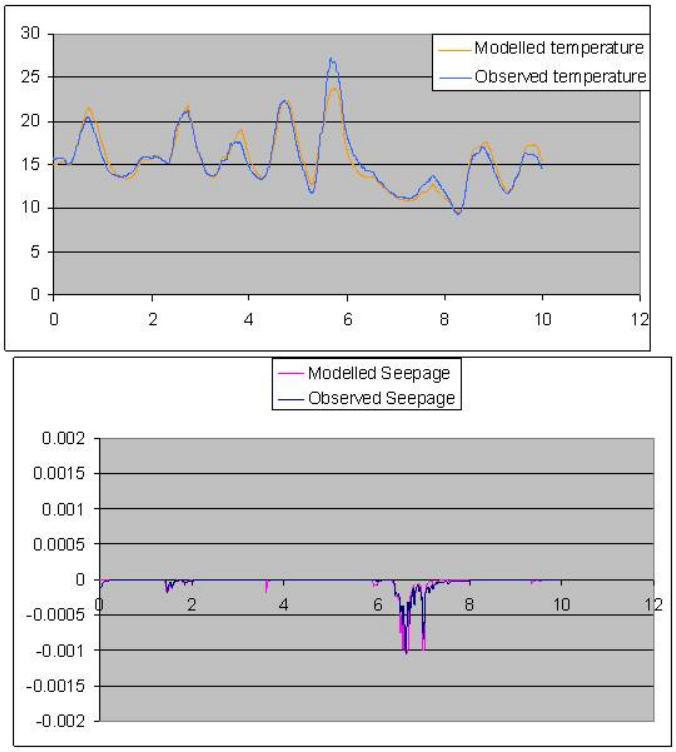

Validation B - 5000